THEORETICAL PREDICTION OF COMPOSITE MODEL ROTOR BLADE STRUCTURAL PROPERTIES USING VARIOUS F.E. MODELLING IDEALISATIONS

S.W.Diamond

Defence Research Agency
Farnborough, England

Abstract

A program of study was initiated to provide a method of theoretical prediction of rotor blade cross-sectional properties in support of the Mach scaled model rotor blade development work in the DRA.

Three methods, all utilising the finite element package MSC/NASTRAN were investigated. Each method involved modelling a thin segment of blade with both faces constrained using multi-point constraint equations. The most suitable method was found to be the representation of each composite ply by a single brick element, although this required significantly more computing time.

A number of FORTRAN pre and post processors were written to automatically produce and analyse finite element composite blade models. Flexibility has been maintained throughout allowing the analysis of a number of methods of blade construction with any reasonable blade profile and with any number of plies of different materials.

Comparison with experimental data has been shown to give good agreement. Predictions of rotor blade parameters which cannot easily be measured experimentally are also available and may be used in conjunction with modes prediction and aeroelastic tailoring programs.

Introduction

The model scale rotor test facility at DRA Farnborough provides the capability to test novel and advanced rotor blades at representative Mach numbers. Current test programs are investigating the implementation and benefits of advanced blade sections and planforms and other concepts. In support of this work, model rotor blades are required to be designed and manufactured to specifications demanding tight tolerances. To aid the design process, an analysis capability is required to calculate rotor blade cross-section properties. These properties characterise the rotor blade in terms of beam elements suitable for data input to rotor analysis programs (Ref 1). Accurate prediction of cross-section properties will accelerate the design process and reduce the number of test samples required before finalising a rotor blade design.

A method for analysing prismatic structures to determine beam type properties, using the finite element method, has been presented by Mercer & Bartholomew (Ref 2). An assessment of the suitability of the method to analyse model rotor blade sections, using FORTRAN programs to generate the required constraint equations and analyse the finite element results, has been produced by Hatch & Lee (Ref 3).

To improve the efficiency of the blade properties prediction method and perform analyses within

the restricted timescales, there is a need to exploit this technique and automate the routine generation of rotor blade finite element models. A number of FORTRAN pre and post processors have been written to automatically generate the complex finite element models and provide a comprehensive rotor blade analysis procedure.

This report considers the typical model rotor blade construction used and compares the different finite element modelling strategies employed to determine the structural properties. An assessment of the relative accuracies of these methods with reference to experimental data is provided. Recommended mesh sizes appropriate for the required level of accuracy are also presented.

Future work is discussed in terms of the overall blade design strategy and philosophy required to establish an increasingly accurate and efficient method of rotor blade design.

Structural Analysis

Programs to predict the performance of helicopter rotors use rotor blade structural information in their analyses in order to perform calculations to the accuracy demanded by current helicopter designs. The rotor blade structural complexity is reduced to a simple beam type representation to ease the task of modelling the blade in an aeroelastic environment. The method adopted by the DRA, for the determination of rotor blade equivalent beam properties is that developed by Mercer and Bartholomew, (Ref 2). This finite element method takes advantage of the 2-dimensional nature of the problem and only models a thin section of the rotor blade to one element deep, making extrusion of the cross-section to a full length blade model unnecessary. This allows for savings in computing resources and enables a very detailed model of the blade cross-section to be analysed and provides results free from end-constraint effects.

A brief resumé of the method is provided here but the reader is referred to reference 2 for a fuller explanation. Examples of NASTRAN data input are contained in reference 3.

It may be seen that the response of a straight, untwisted structure with constant spanwise geometrical and material properties may be adequately characterised by the response of a thin segment bounded by two constant cross-section planes, as shown in Figure 1, (Ref 2). To obtain the response of the full length structure the displacements of corresponding grid points on the two faces of the segment are constrained by the following equations :-

$$u(Q) - u(P) = \mu_1 - \omega_3 \quad (1)$$

$$v(Q) - v(P) = \mu_2 + \omega_3 \quad (2)$$

$$w(Q) - w(P) = \mu_3 - \omega_2 x + \omega_1 y \quad (3)$$

$$rx(Q) - rx(P) = \omega_1 \quad (4)$$

$$ry(Q) - ry(P) = \omega_2 \quad (5)$$

$$rz(Q) - rz(P) = \omega_3 \quad (6)$$

where,

u,v,w	are the translations in the x, y and z directions.
rx,ry,rz	are the rotations about the x, y and z directions.
μ_1,μ_2,μ_3	are the relative rigid body translations between front and rear faces due to the applied loads in the x,y and z directions.
$\omega_1, \omega_2, \omega_3$	are the relative rigid body rotations between front and rear faces due to the applied loads about the x,y and z axes.

The rigid body translations μ_1 and μ_2 are constrained to have zero displacements using single point constraints, SPCs, to fix the rigid body rotations rx and ry. The reaction forces associated with these constraints may therefore be recovered and used later as a measure of the shear loading within the model to enable the position of the shear centre to be calculated, rather than eliminating them from the analysis.

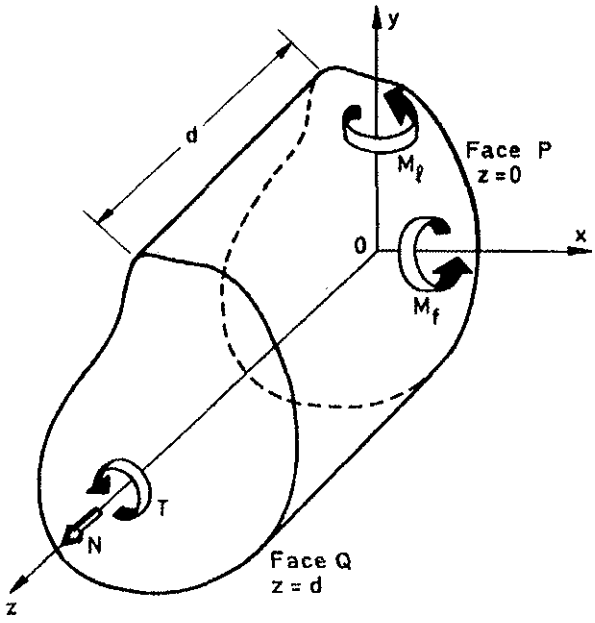

Figure 1; Elemental segment of beam.

In NASTRAN, scalar points specified on the SPOINT card, are used to define the freedoms μ_3, ω_1, ω_2, and ω_3. To define the relative motion between the two corresponding grid points in accordance with the above constraint equations, multi-point constraints (MPCs) are defined which reference the scalar freedoms defined on the SPOINT cards. To satisfy all the above equations some 10 MPC equations are required for each pair of grid points.

The segment is separately loaded with a longitudinal force along the z-direction, flap and lag bending moments and a torque about the z-axis. This is achieved in NASTRAN by applying appropriate scalar loads, using the SLOAD card, to the freedoms μ_3, ω_1, ω_2 and ω_3 by referencing the relevant SPOINT cards previously defined. The SLOAD card applies a uniformly distributed unitary load across the whole cross section, dependent on the freedom referenced. Each loading is specified in a separate subcase and analysed individually.

The flexibility matrix containing the strain vectors derived from the displacement of the scalar freedoms with respect to each of the applied loadings, can be formed from the four separate unit loadings. The flexibility matrix may then be inverted to give the 4 x 4 stiffness matrix the diagonal terms of which are EA the longitudinal stiffness, EI_f stiffness in flap, EI_l stiffness in lag and GJ the torsional stiffness. These are obtained as a direct result from the loading of the freedoms μ_3, ω_1, ω_2 and ω_3. The remaining non-diagonal terms are the stiffness coupling terms essential for work involving aeroelastic tailoring.

The shear centre, the point through which a shear force may be applied without inducing twisting throughout the structure, may also be calculated. A shear force, S, is applied to the beam, without a bending moment, by applying the two shear loadings Sx and Sy obtained from the gridpoint forces NASTRAN output for the ω_1 and ω_2 loaded cases, but with the sense of the front face forces and moments reversed. Again the freedoms μ_1 and μ_2 are constrained to have zero displacement to produce the required loading. The co-ordinates of the shear centre relative to the origin are then given by :-

$$Xs = (GJ\omega_3) / Sy \quad (7)$$

$$Ys = (GJ\omega_3) / Sx \quad (8)$$

where,

Xs is the chordwise shear centre position.
Ys is the shear centre in the y axis.
GJ is the torsional stiffness.
Sx, Sy is the shear loading in the x and y directions obtained from the constrained μ_1 and μ_2 reaction forces.

Modelling Techniques

The global co-ordinate system adopted for all blade models is shown in Figure 2, with the XY plane in the plane of the cross-section and the X axis parallel to the chord of the blade. The model origin is positioned at the leading edge of the blade. The system of ply orientation relative to the blade global co-ordinate system, adopted for all modelling techniques, is presented in Figure 3. The ply orientation of the vertical web is

expressed in a similar fashion but rotated 90 degrees about the Z axis.

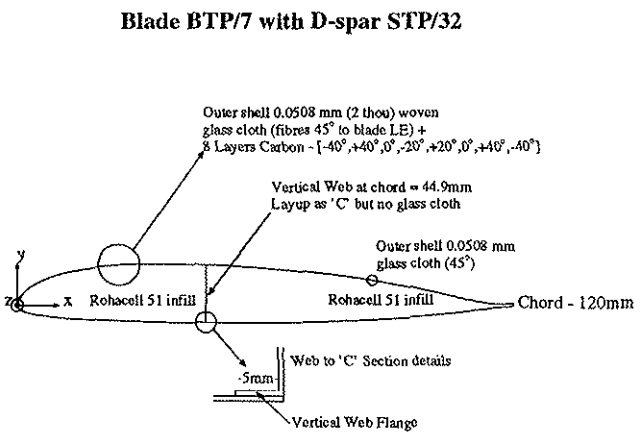

Figure 2; Typical blade test piece.

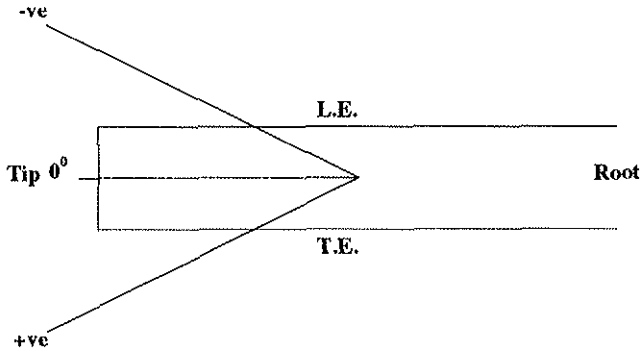

Figure 3; Ply orientation definition.

Three rotor blade modelling techniques were investigated. A brief description of the techniques follows together with analysis results and a summary of their advantages and disadvantages and hence their suitability as a prediction method.

Plate Method

The first method investigated involved the modelling of the 'C-spar' and vertical web shown in Figure 2 using the QUADR plate elements. These QUADR elements maintain a drilling freedom as opposed to the QUAD4 plate elements and do not require freedom suppression and so were thought better suited to the problem. Care was taken to ensure that their utilisation in conjunction with the HEXA foam core brick elements produced accurate results as this procedure is not readily recommended. However, the relatively low stiffness foam core and stiff composite material interface produced no problems and converged results were obtained.

Foam core brick elements possess only translational freedoms and therefore all HEXA associated grid points not connected to a plate element must have rotational freedom suppression specified on the relevant GRID card.

The foam core is meshed in vertical columns linking the top and bottom of the C-spar. Should the elements become too distorted, the meshing processor automatically inserts a five sided PENTA element in place of the six sided HEXA brick element reducing the number of elements in the following column. The foam core is meshed in this fashion for all modelling techniques investigated.

After all grids and elements have been defined, the relative displacements of the two faces of the model are constrained in accordance with reference 2 in the form of multi-point-constraint, MPC cards. Single point constraints, SPC cards are applied to forward and rear points to suppress all translational freedoms of the most forward leading edge point and the 'y' translational freedom of the trailing edge. In this manner the model rigid body motions are suppressed. This multi and single point constraint procedure was performed for all modelling methods investigated.

The outer skin and D-spar composite layers are defined using the PCOMP card. Care was required in defining the order of the QUADR gridpoints as this implies an element co-ordinate system from which the PCOMP properties are referenced. Since the QUADR element uses gridpoint values assigned to the aerofoil profile, offsets must be applied to the PCOMP card to allow for the composite thickness. The default offset indicates a distance equal to half the thickness of the QUADR element and therefore,

without correction, would define an aerofoil profile half the plate element thickness too large.

Material properties for composite elements are defined using the MAT2 card and those of the inner isotropic foam core using the MAT1 card. Material properties used for all three analysis techniques were obtained from manufacturer specifications and are presented in Table 1.

Table 1; Material Properties used in theoretical analyses.

(GPa)	D-Spar Carbon XAS 913	Outer Skin Glass Cloth	Inner Core Rohacell 51 Foam
E1	134.0	14.0	0.07
E2	9.4	19.0	-
E3	9.4	-	-
G12	5.0	4.0	23.5
G13	5.0	-	-
G23	3.3	-	-
ν12	0.26	0.25	0.49
ν13	0.26	-	-
ν23	0.30	-	-
ρ (kg/m^3)	1860	1800	51

Table 2; Plate method theoretical predictions.

Mesh Size (mm)	Flap Stiffness EIf (Nm^2)	Torsional Stiffness GJ (Nm^2)	Shear Centre Xs,Ys (mm from LE)	CG Position (mm from LE)	Mass (kg/m)
Expt	217.0	194.0	28.7, -	0.03	0.383
7.0	212.0	219.5	31.5, 3.4	0.03	0.384
3.0	211.1	218.4	31.4, 3.4	0.03	0.384
2.0	211.0	217.2	31.4, 3.4	0.03	0.384
1.5	211.0	217.1	31.4, 3.4	0.03	0.384
0.75	211.0	217.1	31.4, 3.4	0.03	0.384

Stiffness values predicted using the plate element analysis for blade test specimen BTP/7, defined in Figure 2, are presented in Table 2. The results can be seen to converge at a mesh size of approximately 1.5mm requiring a total of 600 seconds of CRAY2 CPU time for both the stiffness and shear centre calculation model. Good agreement is obtained for the flap bending stiffness EI_F, with theoretical values within 3% of the experimental result, but theoretical torsional stiffness results are approximately 11% too high. A possible contribution to the over-stiffness may be due to the inaccurate plate element representation of the vertical web and C-spar junction and vertical web and web flange junction shown in Figure 2, or plate and brick element interaction problems.

Although absolute theoretical results are only within 11% of the actual experimental results, this technique still provides a very quick method of obtaining approximate results and may be confidently used to study trends observed whilst altering the blade specification or for a lay-up optimisation process.

Brick & Plate Method

The second method modelled both the C-spar and vertical web using HEXA brick elements. It should be noted that each D-spar brick element is the thickness of the whole composite laminate and represents all of the plies. The outer skin material was again represented by QUADR plate elements. HEXA brick elements were used to represent the foam core and constraints were applied as for the previous method.

As one brick element was intended to accurately represent a section of multi-unidirectional, anisotropic composite laminate, care was required in defining the element material properties. An initial stiffness analysis was performed prior to the blade analysis to determine the properties of the laminate as a whole and define the properties for a pseudo material which could then be referenced by each brick element and used to represent the laminate.

A long thin rectangular section composed of HEXA elements one element deep per ply, with material properties and ply orientations identical to the proposed C-spar plies was analysed. The analysis took a similar form to that of a full blade analysis with single and multi point constraints being applied. Laminate stiffnesses were calculated from the scalar displacements due to the scalar loadings. By rotating the global co-ordinate system the laminate stiffnesses and Poisson's ratios in each plane could be calculated, as defined in Figure 4, and used to construct the 6 x 6 stiffness matrix required for the anisotropic MAT9 card to define the

properties of the pseudo material representing the whole laminate. This was referenced by all the HEXA elements representing the C-spar. This procedure was repeated to calculate the stiffness properties of the vertical web laminate which in some cases was composed of a different lay-up. A separate co-ordinate system was defined for each C-spar brick element to account for the rotation about the Z axis as it followed the outer blade profile. Co-ordinate systems are defined using the CORD2R card as described in reference 4.

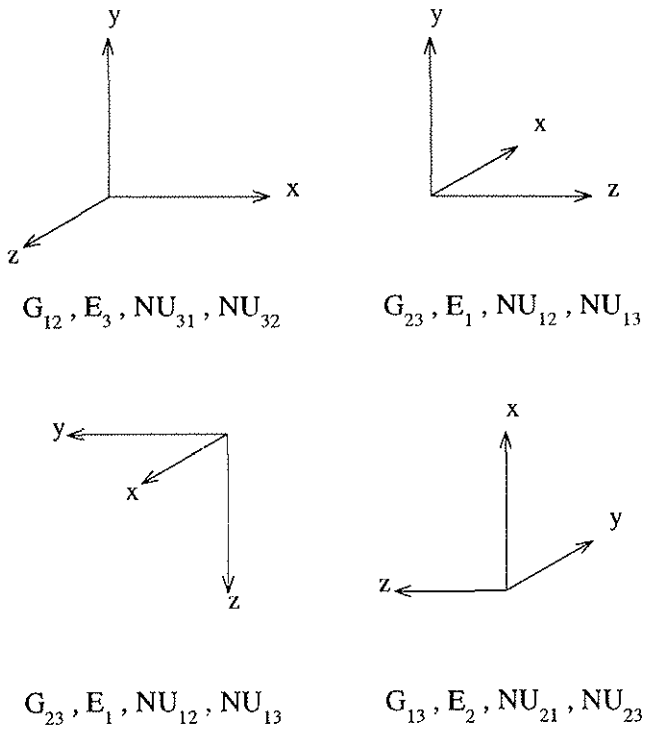

Figure 4; Laminate axis orientation for calculation of various stiffnesses and Poisson's ratios.

The MAT9 card is composed of elements from the 6x6 stiffness matrix calculated from the material properties as shown below, (Ref 5).

$$\begin{bmatrix}\sigma_1\\ \sigma_2\\ \sigma_3\\ \tau_{12}\\ \tau_{23}\\ \tau_{13}\end{bmatrix} = \begin{bmatrix} D_{11} & D_{12} & D_{13} & 0 & 0 & 0 \\ & D_{22} & D_{23} & 0 & 0 & 0 \\ & & D_{33} & 0 & 0 & 0 \\ & & & D_{44} & 0 & 0 \\ & SYM & & & D_{55} & 0 \\ & & & & & D_{66} \end{bmatrix} \begin{bmatrix}\varepsilon_x\\ \varepsilon_y\\ \varepsilon_z\\ \gamma_{xy}\\ \gamma_{yz}\\ \gamma_{xz}\end{bmatrix}$$

where,

$D_{11} = E_x / C_3$, $D_{12} = (C_2/C_1)D_{11}$, $D_{13} = C_4.D_{11}$

$D_{22} = E_y / C_1 + (C_2/C_1)D_{12}$

$D_{23} = \nu_{zy}E_y/C_1 + (C_2/C_1)D_{13}$

$D_{33} = E_z + \nu_{zx}D_{13} + \nu_{zy}D_{23}$

$C_1 = 1 - \nu_{zy}^2(E_y/E_z)$

$C_2 = \nu_{yx} + \nu_{zx}\nu_{zy}(E_y/E_z)$

$C_3 = 1 - (E_x/E_z)\{\nu_{zx}^2 + (E_z/E_y).(C_{22} / C_1)\}$

$C_4 = \nu_{zx} + \nu_{zy}(C_2/C_1)$

The outer skin material properties were defined in a similar manner as in the previous model using the PCOMP card and did not require any co-ordinate system definition. This procedure is not readily recommended but as the outer skin layer was extremely thin and of relatively low stiffness compared to the C-spar laminate, the procedure was adopted.

The results obtained modelling BTP/7 using this method are presented in Table 3. From the converged results at a mesh size of 1.5mm, it can be seen that while the predicted value of flap bending stiffness is within 5% of the experimental value, the predicted torsion stiffness result differs from experimental results by more than 20%. Shear centre results were extremely inaccurate, with the chordwise position being far too close to the vertical web. This may be due to the outer skin plate and C-

spar brick interface or an unknown error in the model.

Table 3; Plate & brick technique theoretical predictions.

Mesh Size (mm)	Flap Stiffness Elf (Nm^2)	Torsional Stiffness GJ (Nm^2)	Shear Centre Xs,Ys mm from LE	CG Position mm from LE	Mass Kg/m
Expt	217.0	194.0	28.7, -	30.0	0.383
3.0	180.8	140.0	39.0, 2.75	-	-
1.5	206.8	150.0	41.0, 2.80	-	-
1.0	204.0	152.0	41.1, 2.85	-	-

The technique of single brick representation was intended to avoid the large detailed blade models required to represent each single ply by a single brick element. However, prior analyses to determine the equivalent stiffnesses of the laminate required long processing times and a great deal of user intervention in the calculation of the final laminate MAT9 values which were hence prone to errors. The method failed to represent the composite laminate suitably and involved the outer skin being modelled using plate elements in conjunction with the C-spar brick elements. This technique of stiff brick and plate element interaction is inaccurate but further effort to model the outer skin elements together with the composite C-spar using a single element was abandoned as this entire method was thought unsuitable. This technique has therefore proved to be unsuitable for rotor blade cross-sectional stiffness prediction and so a third technique was investigated.

Brick / ply method

The final method investigated involved representing each composite ply by an 8 noded HEXA brick element. This method required much larger models with complicated mesh transitions and a large number of co-ordinate systems to define ply orientations and account for the Z axis rotation about the aerofoil profile. This resulted in models demanding much larger CPU times for each blade analysis.

Prior to investigating this method, a simple feasibility study was conducted. As the thin outer skin would have to be modelled using HEXA brick elements, the element aspect ratios would have to be reduced by using a very fine mesh hence dictating the aspect ratios of the inner C-spar elements. To determine how fine this mesh would be required to be and in turn determine if this method would prove to be a viable option, long composite rectangular brick element spar models with identical external dimensions were generated with different element aspect ratios as shown in Figure 5. These were then analysed along with identical plate element models. It can be seen from the results shown in Figure 6 that no significant loss in accuracy is incurred due to element aspect ratio increase. Results differ by approximately 1.5% between models composed of aspect ratio 2 elements and aspect ratio 20 elements which was regarded as being acceptable.

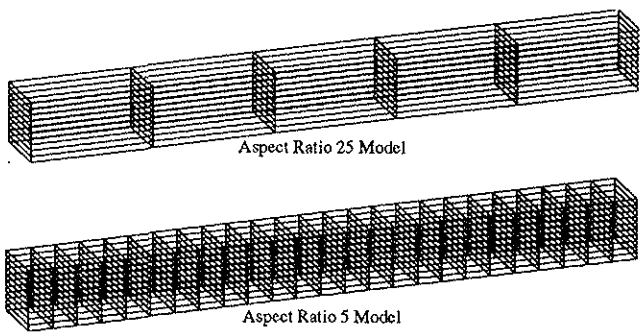

Figure 5; Beam models for determination of suitable element aspect ratios.

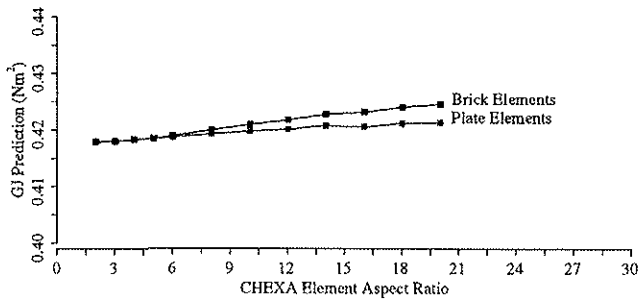

Figure 6; Stiffness predictions of beams with varying element aspect ratios.

A box structure, with four corner junctions each similar to the C-spar & Vertical web junctions,

composed of composite material with an isotropic foam core, as shown in Figure 7, was analysed and again the effect of varying element aspect ratios observed. This analysis would be subject to the same problems as a blade model and it can be seen from the torsional stiffness results presented in Figure 8 that models with element aspect ratios of 20 differ from aspect ratio 2 models by less than 0.5%. The larger aspect ratio models are therefore acceptable. Flap stiffness results were identical for all models analysed. From this feasibility analysis it was deduced that a full blade model with a mesh size of 1mm would provide converged results to an acceptable accuracy. This method of modelling was regarded as being feasible and was pursued.

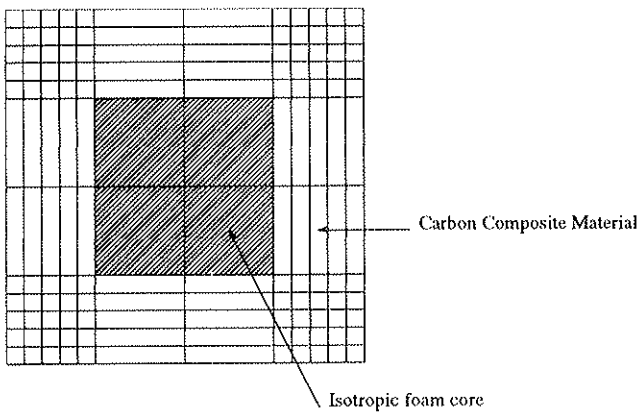

Figure 7; Box structure representative of vertical web and flange junction.

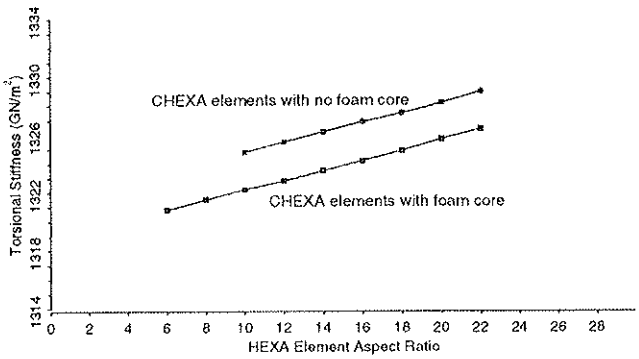

Figure 8; Torsional stiffness predictions of box structure with varying element aspect ratio.

As with both previous methods single point and multi-point constraints were enforced. The carbon composite and skin woven cloth material properties were specified using the MAT9 card. The inner isotropic foam core properties were defined using the MAT1 card.

A simplified example of the complicated meshing of the vertical web and vertical web flange junctions is shown in Figure 9. The mesh transitions between these junctions and the Rohacell core have been omitted for model simplicity and foam HEXA elements are only attached to composite vertical web elements at the upper ply and lower ply corners of the laminate. This results in a slightly inaccurate strain distribution across the surface of the adjoining foam element but comparisons of models with a transitioned mesh to those non-transitioned suggest no significant inaccuracy is incurred, Table 4.

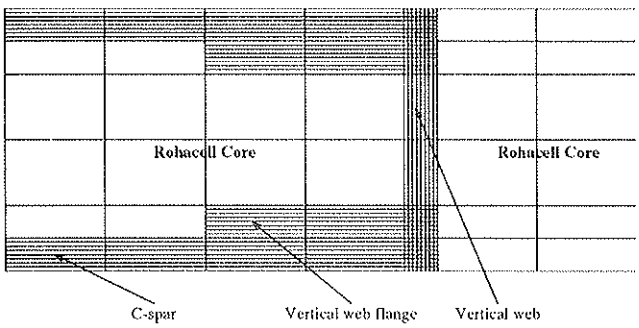

Figure 9; Simplified diagram of vertical web and C-spar modelling.

Table 4; Brick/ply method theoretical predictions.

Mesh Size (mm)	Flap Stiffness EIf (Nm²)	Torsional Stiffness GJ (Nm²)	Shear Centre Xs,Ys mm from LE	CG Position mm from LE	Mass (kg/m)
Expt	217.0	194.0	28.7, -	0.03	0.384
2.0	214.7	188.0	27.3, 3.3	0.03	0.385
1.5	215.2	189.5	27.3, 3.3	0.03	0.385
1.0	214.9	189.3	27.3, 3.3	0.03	0.385
1.0*	214.9	189.3	27.3, 3.3	0.03	0.385
1.0**	214.3	189.4	27.3, 3.3	0.03	0.385

* Transitioned mesh
** Coarse foam mesh (every 5th node meshed)

From the results presented in Table 4, it can be seen that a convergence is achieved at a mesh size of approximately 1mm. Results are very

encouraging with predicted flap bending stiffness results within 1% of experimental results and shear stiffness results within 2.5% although at a mesh size of 1.0mm a total of approximately 7800 seconds of CRAY2 CPU time is required for both runs. However, since this investigation began DRA has access to the CRAY YMP which has cut the analysis time by 75% for all modelling techniques giving acceptable run times.

Using the model generation program 'BLADE', a variable may be defined such that the foam core elements are connected to the spar elements in a stepped fashion, i.e. a specified number of C-spar nodes are skipped, dramatically reducing the number of relatively unimportant foam core elements required to specify the model. Coarse foam mesh results from models analysed in this manner are presented in Table 4 and may be seen to be almost identical to the full blade results but reducing CPU time by approximately one third at finer mesh sizes. Shear centre results are within experimental error of ±2.5% and centre of gravity and mass predictions agree with measurements.

A number of other full section composite blades and D-spars with different lay-ups were modelled and analysed using this technique. From the theoretical and experimental results contained in Table 5 it can be seen that stiffness predictions are generally within 5% of experimental results suggesting that this technique is reliable.

The technique of representing each ply by one brick element provides results which compare favourably with experimental data and provides a greater degree of modelling flexibility. This method, although longer with regard to CPU time, is the more appropriate of the three and may be used confidently as a tool in the design of composite model rotor blades.

Table 5; D-spar and full blade theoretical predictions using brick/ply technique.

D-Spar	Experimental			Theoretical		
	Elf (Nm^2)	GJ (Nm^2)	Xsc (mm)	Elf (Nm^2)	GJ (Nm^2)	Xsc (mm)
STP/27	157.0	156.0	26.8	155.0	170.6	27.6
STP/28	158.0	164.0	26.8	155.0	170.6	27.6
STP/29	144.4	147.0	-	141.7	155.0	27.7
STP/31	246.0	151.0	26.6	239.6	150.3	26.7
STP/32	208.0	175.5	-	200.5	178.9	26.1

Blade	Experimental			Theoretical		
	Elf (Nm^2)	GJ (Nm^2)	Xsc (mm)	Elf (Nm^2)	GJ (Nm^2)	Xsc (mm)
BTP/7	217.0	194.0	28.7	214.9	189.3	27.3
BTP/9	258.0	245.0	30.0	267.0	238.0	31.0
BTP/11	251.0	239.0	30.0	265.0	232.0	30.9
BTP/12	200.0	80.0	-	188.0	77.5	17.7
BTP/21	270.0	164.2	31.5	277.3	172.7	31.9
BTP/24	271.5	171.0	31.5	277.3	172.7	31.9

Discussion of Modelling Techniques

A number of advantages and disadvantages are associated with each of the modelling techniques presented. The first method provides a simple, quick method of producing a representative blade model and obtaining reasonably accurate results. However the models are not spatially representative of the actual blades as a solid region in the XY plane is being represented by a thin plate element and consequently an area which should be occupied by the composite material is represented by Rohacell foam. This does not present a significant problem when the inner core material is much less stiff than that of the spar, as with the Rohacell core, but it would prove significant if another more substantial material were to be used.

The second method adopted in an attempt to avoid this problem, has proved very unsuccessful. It was intended that the complications associated with the one brick per ply models would be avoided, however due to the complicated process of determining laminate stiffness properties used in the MAT9 card, this process proved time consuming and failed to accurately represent the laminate. Consequently, unreliable results were obtained from the full blade model analyses and often convergence of

results with decreasing mesh size could not be achieved.

The third technique, consisting entirely of HEXA brick elements is the most spatially representative method and as expected provides the most accurate results. This method is also the most flexible for modelling future alterations to blade construction, as spatial representation is not compromised. The use of HEXA elements to represent the entire blade structure avoiding the combination of different elements, prevents element interaction problems which have previously been encountered. Another advantage of using this method is that ply stresses, strains, strain energy etc. are available and may be graphically displayed in detail using existing FORTRAN post- processors and the graphics package MSC/XL. The only disadvantage associated with this modelling procedure is the very large amount of data required to define a model with a suitable mesh size to ensure that the element aspect ratios are sensible. However this problem has been largely overcome with the use of the faster CRAY YMP.

It should be noted, for all modelling techniques employed to analyse rotor blade sections, that predicted cross sectional absolute values may not be extremely accurate compared to the experimental results. Emphasis should, however, be placed upon the trends whilst modifying the blade design as it is these that may be effectively used to aid the blade design process and reduce the number of blade samples required.

Comparing the results from all techniques explored, the brick per ply method has been adopted by the DRA as an established method of blade analysis for the design of model rotor blades for testing on the new 5m Wind Tunnel Rotor Rig.

Future Work

A powerful, 'user-friendly' system of blade analysis has now been established within the DRA. As this system is used as a tool in the design of model rotor blades and more experimental data becomes available, discrepancies between experimental and theoretical data due to inaccurate material property definition or modelling techniques may be identified and improved upon.

Further work may be carried out in the way of an optimisation process, possibly incorporating a sensitivity analysis already existing within the NASTRAN code. This may be used again to reduce the number of test pieces required and may prove useful in achieving the tight design requirements necessary in the work within this field.

Conclusions

Three different methods of modelling rotor blade cross-sections, all utilising the finite element package MSC/NASTRAN, have been investigated.

The method of representing each composite ply with a single brick element has proved to be the most accurate representation of the blade.

A comprehensive method of blade analysis has been established which accurately represents any model D-spar constructed rotor blade. The method provides reliable results and through the use of in-house pre and post processors may be performed by a user with limited knowledge of composite theory and finite element analysis to predict rotor blade cross-sectional properties.

References

1 Juggins, P.T.W. *A Comprehensive Approach to Coupled Rotor-Fuselage Dynamics.* Westland Helicopters Ltd. Paper No. 48, Fourteenth European Rotorcraft Forum. Milano, Italy.

2. Mercer A.D. & Bartholomew P. *Analysis of an Anisotropic Beam with Arbitrary Cross-section.* RAE Technical Report 84058 (1984) UNCLASSIFIED

3. Hatch C. & Lee A.R. *Determination of the Structural Properties of Helicopter Rotor Blades by Theoretical and Experimental Methods.* Paper No. 67 Twelfth European Rotorcraft Forum, September 1986.

4. The MacNeal Schwendler Corporation. *MSC Version 64, Handbook for Linear Analysis.*

5. Brebbia CA. *Fundamentals of Finite Element Techniques for Structural Engineers* J.J.Connor. Butterworths.

6. Wei-Liang W., *Mechanical Properties of Warp-Knitted Fabric Reinforced Composites.* Journal of Plastics and Composites. Vol.12. October 1993.

7. Chan W.Y.F. *Evaluation of Composite Blade Structural Properties Using Finite Element Method.* Westland Helicopters Ltd. Internal Dynamics Department Report. December 1985